catalysts

MDPI

Article

Assessing the Degradation of Levofloxacin in Aqueous Media by Metal-Free g-C_3N_4 Photocatalyst Under Simulated Solar Light Irradiation

Truong Nguyen Xuan [1], Dien Nguyen Thi [2], Cong Le Thanh [2], Thu Mai Thi [2], Thu Le Dieu [1], Trung Nguyen Duc [1] and Ottó Horváth [3,*]

[1] School of Chemistry and Life Sciences, Hanoi University of Science and Technology, No. 1 Dai Co Viet Street, Hai Ba Trung District, Hanoi 100000, Vietnam; truong.nguyenxuan@hust.edu.vn (T.N.X.); thu.ledieu@hust.edu.vn (T.L.D.); trung.nguyenduc1@hust.edu.vn (T.N.D.)
[2] Viettel Aerospace Institute, Viettel Group, Hoa Lac High-Tech Park, Thach That District, Hanoi 10000, Vietnam; diennt15@viettel.com.vn (D.N.T.); conglt14@viettel.com.vn (C.L.T.); thumt6@viettel.com.vn (T.M.T.)
[3] Research Group of Environmental and Inorganic Photochemistry, Center for Natural Sciences, Faculty of Engineering, University of Pannonia, P.O. Box 1158, H-8210 Veszprém, Hungary
* Correspondence: horvath.otto@mk.uni-pannon.hu; Tel.: +36-88-624-000 (ext. 6049)

Abstract: Graphitic carbon nitride (g-C_3N_4) as a fascinating conjugated polymer has attracted considerable attention due to its outstanding electronic properties, high physicochemical stability, and unique structure. In this work, we reported the characterization of g-C_3N_4, which was simply synthesized by thermal polymerization of thiourea, the photocatalytic degradation kinetics, and the pathway of levofloxacin (LEV) using the prepared g-C_3N_4. The XRD and SEM results confirmed a crystalline graphite structure with a tri-s-triazine unit and stacked sheet-like layers of g-C_3N_4. The efficacy factor (EF) was compared to different photocatalytic processes to assess the LEV removal performance. g-C_3N_4 exhibits good stability as a photocatalyst during LEV photodegradation. Radical scavenger experiments revealed that in the oxidative degradation of LEV, $^{\bullet}O_2^-$ and h^+ played the determining roles. Moreover, based on the identification of intermediates using liquid chromatography with tandem mass spectrometry (LC-MS/MS), the degradation pathway of LEV was proposed.

Keywords: antibiotics; pH-effects; adsorption; kinetics; mechanism; radical scavenging; intermediates

Citation: Xuan, T.N.; Thi, D.N.; Thanh, C.L.; Thi, T.M.; Dieu, T.L.; Duc, T.N.; Horváth, O. Assessing the Degradation of Levofloxacin in Aqueous Media by Metal-Free g-C_3N_4 Photocatalyst Under Simulated Solar Light Irradiation. *Catalysts* **2024**, *14*, 837. https://doi.org/10.3390/catal14110837

Academic Editors: Albin Pintar and Gregor Žerjav

Received: 21 October 2024
Revised: 12 November 2024
Accepted: 17 November 2024
Published: 20 November 2024

1. Introduction

Antibiotics have been widely used in all aspects of human life against infectious diseases. The existence of antibiotics in diverse environments is harmful to human health due to their potential toxicity, carcinogenicity, mutagenicity, and endocrine disruption. Currently, more and more cases are resistant to antibiotics, which hinders the treatment process [1,2]. This is due to many different reasons, but one of the main reasons why bacteria are resistant to specific drugs, making them ineffective when used in humans, is antibiotic pollution [3–5].

Levofloxacin (LEV) is classified as a third-generation quinolone. It is active against both Gram-positive and Gram-negative bacteria and is used in the treatment of many diseases, including urinary, respiratory, and gastrointestinal tract infections [6–8]. LEV is excreted as unchanged drug mainly in the urine (>80% of the dose) [9]. With its complex molecular structure, high stability, and low biodegradability, LEV removal has received increasing attention. To date, photocatalysis has become a promising process for the removal of LEV in water [10–18]. This method utilizes abundant solar energy, and avoiding secondary pollution is considered a friendly environmental solution.

g-C_3N_4 is a popular metal-free semiconductor with an appealing electronic band structure and high physicochemical stability. Moreover, g-C_3N_4 has many advantages, such as an average band gap energy (E_g) value of ≈2.7 eV to aid the visible light absorption, low cost, and facile preparation, promising for photocatalytic applications. These properties make it conspicuous among other metal oxides, for example TiO_2, ZnO and SnO_2. g-C_3N_4 is synthesized from nitrogen-rich precursors such as urea [19], melamine [20], cyanamide [21], and dicyandiamide [22]. The common methods used for the preparation of g-C_3N_4 are thermal polymerization [23], hydrothermal [24], and sol-gel [25]. In this study, g-C_3N_4 was synthesized by thermal polymerization of thiourea calcining at 550 °C. The morphology, structure, and optical properties of the prepared photocatalysts were described and analyzed in detail. The kinetics and optimization of experimental parameters (initial pH value, catalyst content and initial LEV concentration) for photocatalytic degradation of LEV and the reusability of the photocatalyst were also reported. To assess the LEV decomposition efficiency by the g-C_3N_4 photocatalyst, the efficacy factor was calculated. Furthermore, the identification of intermediates was analyzed to propose the LEV degradation mechanism. Although g-C_3N_4 modified with various dopants, metal depositions or combined with other photocatalysts forming composites or Z-schemes were applied for the degradation of LEV without additional oxidants or in the presence of peroxomonosulfate [26–30], unmodified g-C_3N_4 has not been used so far for this purpose. Additionally, a systematic study involving pH-effects, adsorption, kinetics, and mechanistic investigation has not been made with this photocatalyst−pollutant combination; hence, these results serve useful comparisons, too.

2. Results and Discussion

2.1. Characterization

2.1.1. XRD Analysis

The XRD spectroscopy of g-C_3N_4 is shown in Figure 1. It can be seen the presence of two peaks corresponds to the graphite structure with a tri-s-triazine unit [3,31,32]. The sharp peak at 27.3° is attributed to the interplanar stacking of aromatic systems, which can be indexed to the (002) crystal plane [19,20]. The small peak at 13.2° is related to the cyclic arrangement of the condensed tri-s-triazine unit in the structure, which could be indexed to the (001) plane (JCPDS No. 87-1526) [21–23]. Broad and weak reflections at approximately 2θ = 17.7° and 2θ = 21.9° are typical of melamine. It can be reasonably hypothesized that a network of hydrogen-bonded melamine/triazine units is present inside the heptazine framework [33].

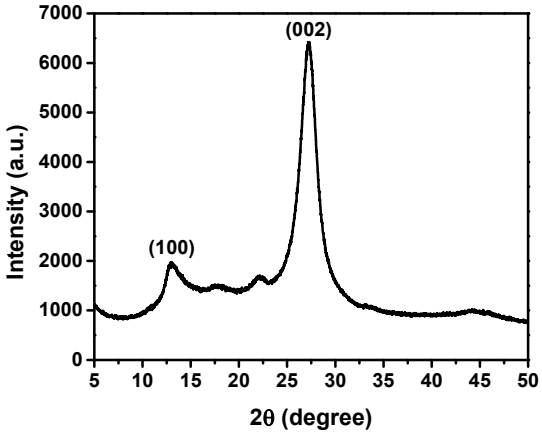

Figure 1. XRD pattern of g-C_3N_4 catalyst.

2.1.2. SEM Analysis

As can be seen in Figure 2, the morphology of g-C_3N_4 consists of stacked sheet-like layers. The sizes of the plates are not uniform and agglomerate together into a block.

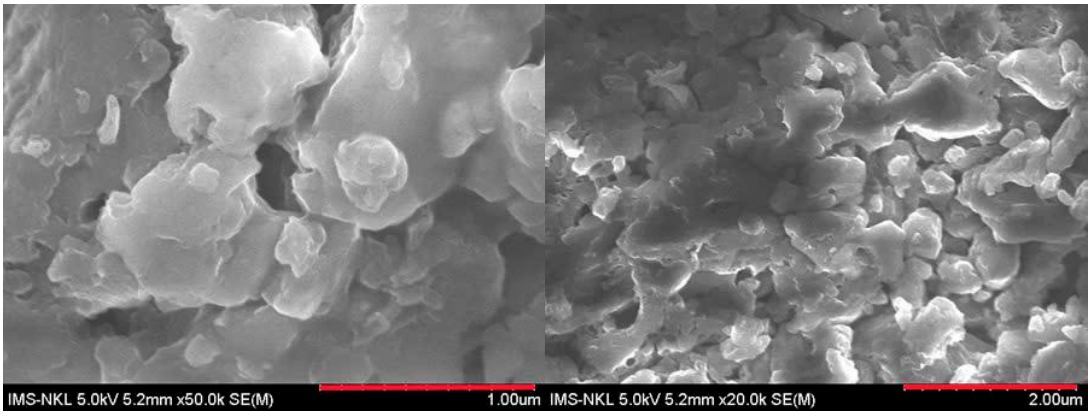

(**a**) (**b**)

Figure 2. SEM images of g-C_3N_4 catalyst with different resolutions. (**a**) 50,000× magnification, (**b**) 20,000× magnification.

2.1.3. Optical Measurements

Absorption spectroscopy was applied to study the optical properties of the synthesized sample, which can play important roles in the photocatalytic behavior. Figure S1 shows the UV-Vis diffuse reflectance spectra and the Tauc plot [34] of the g-C_3N_4 sample. The latter one indicates the band gap (E_g), which was determined to be 2.60 eV for the prepared g-C_3N_4. This is in good accordance with the value measured in our previous work [35,36]. Using the band-gap energy, the edge potential of the conduction band (CB) and valence band (VB) can be estimated by application of the following equations (Equations (1) and (2)) [17]:

$$E_{CB} = E_{VB} - E_g \quad (1)$$

$$E_{VB} = \chi - E_e + 0.5E_g \quad (2)$$

where χ designates the Mulliken electronegative symbol of g-C_3N_4 (4.73 eV [37]), while E_e represents the energy of free electrons on the hydrogen scale ($E_e \approx 4.50$ eV, [38]). Thus, E_{VB} estimated for this semiconductor is 1.53 eV, while E_{CB} is −1.07 eV. The latter is far more negative than the potential needed for the reduction of O_2 to $^{\bullet}O_2^-$ (−0.16 eV [39]). However, the edge potential of VB seems to be rather low for the oxidation of H_2O or OH^- to $^{\bullet}OH$, considering the corresponding redox potential (2.27 eV, [27]). On the basis of these results, one would expect that in the degradation of LEV in this work, hydroxyl radicals cannot play determining roles, while superoxide is a good candidate for that, and the valence-band holes can also be taken into consideration in this respect.

2.2. Optimization of the Experimental Conditions for LEV Photodegradation in Solution

2.2.1. Effect of Initial Solution pH Value

The initial pH value of the solution plays an important role in the photodegradation of antibiotics. According to previous studies, pH can affect the LEV removal ability of the catalyst [40–42]. The influence of pH media on LEV treatment with g-C_3N_4 was studied, and the results are illustrated in Figure 3.

When the initial solution pH value increased from 3 to 5, the LEV removal efficiency (H%) exhibited an extreme increase from 36.3% to 80.1%, and the corresponding k value increased from 0.006 min^{-1} to 0.021 min^{-1}. As the pH values changed from 5 to 10, the LEV degradation efficiencies decreased from 80.1% to 41.9% and the corresponding k-values decreased from 0.021 min^{-1} to 0.008 min^{-1}. These results suggest that neutral or weakly acidic media are better for the LEV removal, while strong acid or strong basic conditions hinder the catalytic degradation performance. In accordance with the degradation rates, the efficiency of the adsorption of LEV on the surface of the catalyst particles shows a similar tendency upon changing the initial pH (see the "dark" range of Figure 3a).

This confirms that adsorption of is strongly correlated with the rate and efficacy of the photocatalytic degradation.

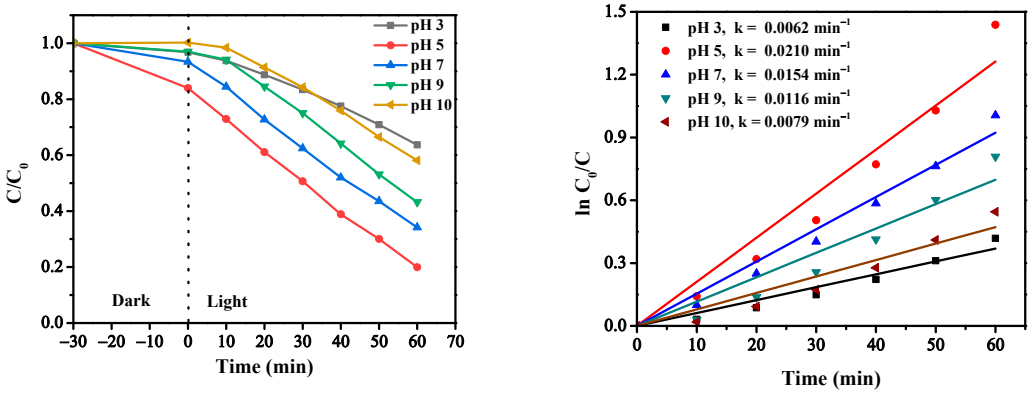

(**a**) (**b**)

Figure 3. (**a**) Effect of initial solution pH on the photocatalytic activity and (**b**) first-order kinetic curves.

The above results can be explained by the following aspects. First, the dissociation state of the pollutant and the surface charge of the catalyst vary with pH. As is known, levofloxacin has two dissociation constants: 6.02 (pK_{a1}) and 8.15 (pK_{a2}), which means that levofloxacin exists as LEV^+ cation (pH < 6.02), $LEV^{\pm}$ neutral state (in the pH range 6.02–8.15) and LEV^- anion (pH > 8.15) [10,41]. In addition, g-C_3N_4 exhibited a zero charge point (pH_{pzc}) around 6.97 (Figure 4), indicating that the catalyst surface is positively charged at pH < 6.97 and negatively charged at pH > 6.97. Hence, electrostatic repulsion between LEV and g-C_3N_4 may occur due to their uniform charge characteristics under extreme acidic or alkaline conditions, which restrained the contact between the catalysts and the contaminants, thus reducing the catalytic efficiency [11,41].

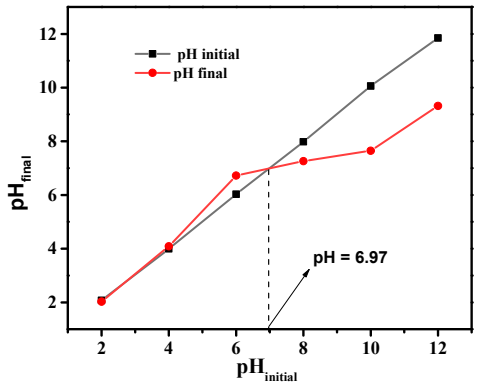

Figure 4. pH_{pzc} determination for g-C_3N_4.

The generation of reactive oxygen species, which include superoxide anion radicals ($^{\bullet}O_2^-$), hydroxyl radicals ($^{\bullet}OH$), hydroperoxyl radicals ($^{\bullet}HO_2$), and hydrogen peroxide (H_2O_2), during the photocatalytic process may be another important factor that accounts for the change of LEV removal efficiency with pH. At higher pH, a large amount of OH^- ions are present on the surface of the catalyst, which facilitates the formation of $^{\bullet}OH$. When reaching strong alkalinity (pH 10), excess $^{\bullet}OH$ and LEV molecules will compete for adsorption on the surface of g-C_3N_4, thus reducing the adsorption amount of LEV molecules on the surface of g-C_3N_4, resulting in a reduction in photocatalytic degradation efficiency [41]. With a pH environment near pH_{pzc}, the surface of the material is almost uncharged and practically unaffected by the electrostatic repulsion that occurred between g-C_3N_4 and LEV. LEV primarily appeared as a zwitterion as the pH value increased to

neutral, making active species attack easier [12]. Therefore, pH 5 with the highest catalytic treatment efficiency was selected as the optimal pH in this experiment.

The results of the effect of photolysis on the degradation of LEV pollutants at pH 5, are depicted in Figure 5. Without the use of a photocatalyst, the photolysis experiment was carried out under the same reaction conditions (pH 5, and 10 mg/L concentration of LEV). The results showed that solar light irradiation did not significantly affect the degradation of LEV (H = 6.5%), indicating that its absorption in the UV range results in only a slight decomposition. An experiment using g-C_3N_4 photocatalyst was carried out in the dark with optimal reaction conditions to investigate the impact of adsorption on the removal of the LEV drug. In the dark, a small amount of LEV adsorption was observed, indicating that adsorption was not a main factor for the removal of LEV (H = 16.0%). A noticeable degradation of LEV was seen when a solution of LEV-containing photocatalyst was exposed to solar light. It is evident from Figure 5 that photocatalysis played a major role in the degradation of LEV (H = 80.1%).

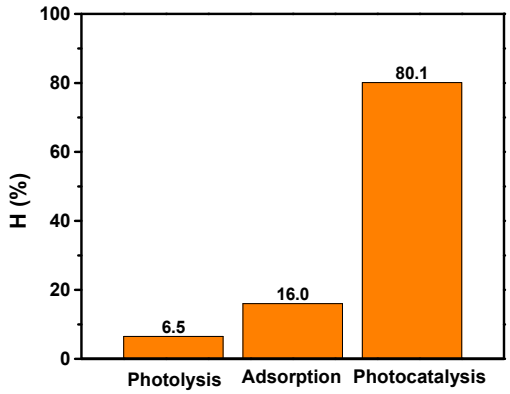

Figure 5. Comparison between photolysis, adsorption and photocatalysis by g-C_3N_4.

2.2.2. Effect of Photocatalyst Concentration

The effect of catalyst dose on the degradation of LEV was investigated using five different doses of g-C_3N_4 composite (i.e., 0.1, 0.2, 0.5, 0.7 or 1.0 g/L) in 100 mL LEV (10 mg/L) at pH 5. The results are shown in Figure 6, which shows that the degradation efficiency of LEV improved with increasing the catalyst dose. As shown in Figure 6, the corresponding removal rate constants at different catalyst concentrations were 0.0074, 0.0140, 0.0210, 0.0283 and 0.0251 min^{-1}. The effect of catalyst dosage can be explained by the following reasons. Increasing the amount of catalyst results in a higher number of active sites and a higher density of catalyst particles in the illuminated area. Therefore, the photocatalytic capacity of the material is improved, resulting in faster decomposition [43]. However, if the catalyst content is continuously increased, it may lead to an excessive density of particles suspended in solution, which hinders light penetration and promotes the light scattering effect (i.e., prevents light absorption during the reaction). Consequently, further increasing the catalyst dosage (1.0 g/L) did not lead to an improvement in photocatalytic performance. Therefore, a dose of 0.5 g/L was optimal for photodegradation of LEV in 60 min.

2.2.3. Effect of Initial LEV Concentration

The influence of the original LEV concentration on the photocatalytic efficiency is displayed in Figure 7. With the increase of LEV concentration from 5 mg L^{-1} to 20 mg L^{-1}, the removal efficiency of LEV gradually declined from 83.62% to 43.17% within 60 min irradiation, and the corresponding k value decreased from 0.0305 min^{-1} to 0.0073 min^{-1}. Clearly, the higher initial LEV content had a negative impact on the catalytic behavior of the g-C_3N_4 photocatalyst. The reduction in removal efficiency might be derived from the fact that the limited number of reactive species produced at the catalytic system was insufficient to attack the excess pollutants. When the LEV concentration is increased, the photons are blocked before reaching the catalyst surface, causing a lower amount of $^{\bullet}OH$ and $^{\bullet}O_2^-$

radicals (the photogenerated electrons react with the dissolved O_2 on the surface of g-C_3N_4 and transform to $^{\bullet}O_2^-$), meaning the removal efficiency is decreased [44]. Besides, the higher LEV content would block the penetration of visible light and cover the active site of the catalyst, subsequently inhibiting the formation of the active species [42]. Simultaneously, as the initial LEV concentration increased, more and more complex intermediates might be generated in the reaction system, which would also compete with the target pollutant for constant active species, resulting in a decrease of LEV photodegradation. Nevertheless, if we take the absolute rate into account, multiplying the rate constant with the corresponding initial concentration, the highest value is obtained for the 10 mg L^{-1} concentration (0.210 mg L^{-1} min^{-1}). The absolute rate moderately decreased at higher concentrations, but even at 20 mg L^{-1}, it just slightly dropped below that observed for the 5 mg L^{-1} concentration (0.146 vs. 0.153 mg L^{-1} min^{-1}). It means that the hindering effects described above are overcompensated by the increase in the rate due to the higher concentration in most of the range studied.

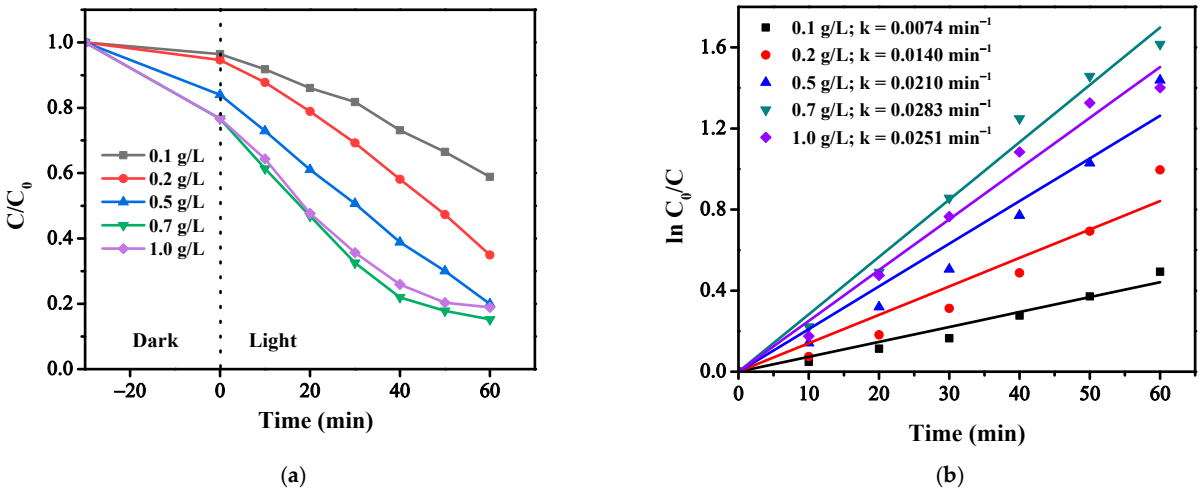

Figure 6. (**a**) Effect of photocatalyst content on the photocatalytic activity and (**b**) first-order kinetic curves.

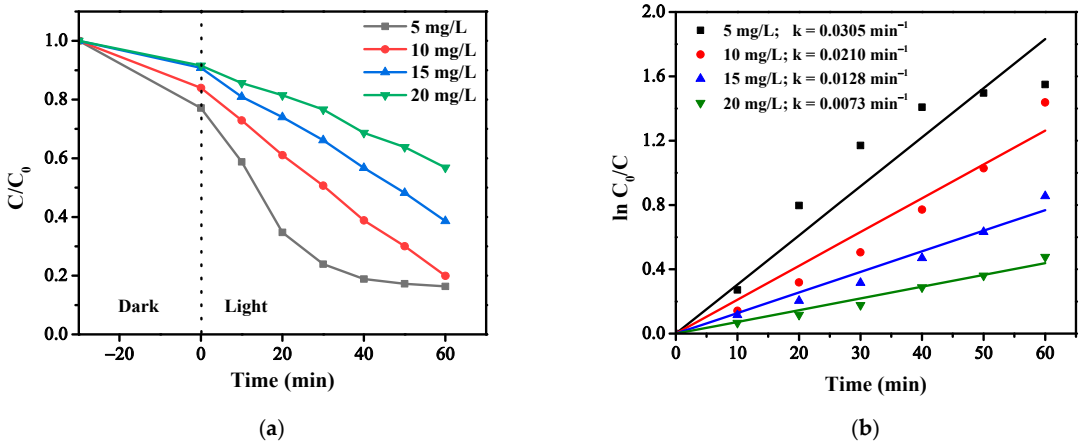

Figure 7. (**a**) Effect of initial LEV concentration on the photocatalytic activity and (**b**) first-order kinetic curves.

2.3. Efficacy Factor of the Photocatalyst

The efficacy factor (EF), which describes the number of contaminants eliminated per concentration of catalyst per treatment time, is used to assess the LEV removal per-

formance by different photocatalytic processes. The EF calculation formula is given as Equation (3) [45]:

$$\mathrm{EF} = \frac{\text{Concentration of LEV (mg/L)} \times \text{\% of its reduction}}{\text{Catalyst concentration (mg/L)} \times \text{time (min)}} \quad (3)$$

From the results of optimized experimental conditions, the performance factor was calculated to compare the photoactivity of reported catalysts for LEV removal. The calculated results are shown in Table 1.

Table 1. Comparison of different photocatalytic processes for degradation of LEV.

Photocatalyst	Catalyst (g/L)	LVFX (mg/L)	Removal (%)	Time (min)	EF	Ref.
g-C_3N_4	0.5	10	80.1	60	2.67×10^{-4}	This study
$CaTiO_3$/g-C_3N_4	0.2	20	87.7	120	7.31×10^{-4}	[13]
Co/Fe-CN-PMS	0.4	20	92.1	50	9.21×10^{-4}	[11]
TOB CN (1-3)	0.2	10	99.2	50	1.98×10^{-4}	[46]
BiOCl/g-C_3N_4	0.25	10	94.2	150	2.51×10^{-4}	[47]
Cu (0)/PCN	1.0	15	98.2	60	2.45×10^{-4}	[14]

The results in Table 1 show that the metal-free g-C_3N_4 photocatalyst has a relatively good EF coefficient and can be used as a potential catalyst for treatment of LEV. On the other side, if the pure g-C_3N_4 is modified by doping metal oxides (ex. $CaTiO_3$/g-C_3N_4), co-doping metals, and adding a strong oxidizer (ex. Co/Fe-CN-PMS), its catalytic activity will be improved.

2.4. Reusability of the Photocatalyst

The reusability of the g-C_3N_4 photocatalyst was evaluated over four consecutive cycles. It can be seen from Figure 8 that a lower degradation rate was obtained after recycling. Within 60 min of irradiation, the photocatalytic performance was reduced from 80.1% to 49.0% after three reuses. This can be explained by a slow recovery of the active sites on the catalyst. It may require a longer time for the g-C_3N_4 photocatalyst to reach its overall original efficiency.

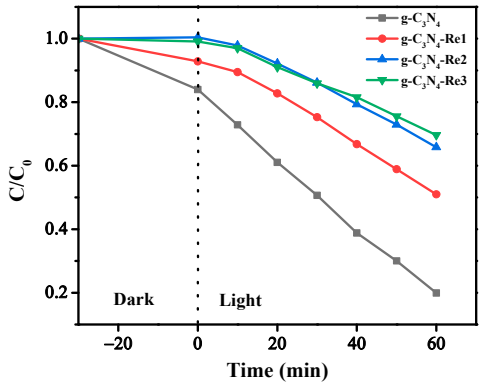

Figure 8. Recycle experiments of the LEV degradation using g-C_3N_4 photocatalyst.

2.5. Radical Trapping

Oxidizing agents such as $^{\bullet}O_2^-$, $^{\bullet}OH$, h_{VB}^+ formed during photocatalysis are considered to play important roles in levofloxacin degradation. To elucidate the photodegradation mechanism, the effects of various reactive oxidative species (ROS) on the decomposition of levofloxacin over g-C_3N_4 were investigated. In this photocatalytic study, isopropyl alcohol (IPA), benzoquinone (BQ), and ammonium oxalate (AO), were employed to capture hydroxyl radicals ($^{\bullet}OH$), superoxide ($^{\bullet}O_2^-$,) and holes (h^+) as reactive species in photo-

catalytic process, respectively. The photocatalytic decomposition of levofloxacin in the presence of the radical trapping agents is shown in Figure 9.

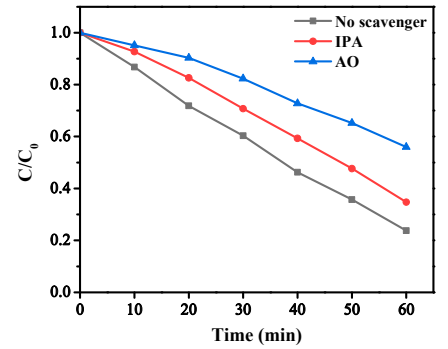

(**a**)

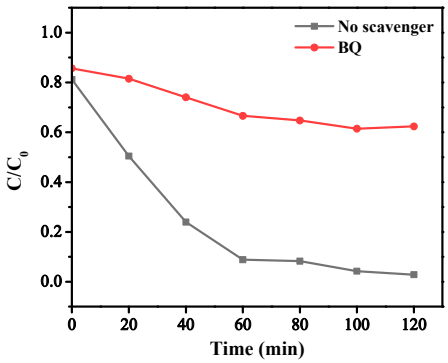

(**b**)

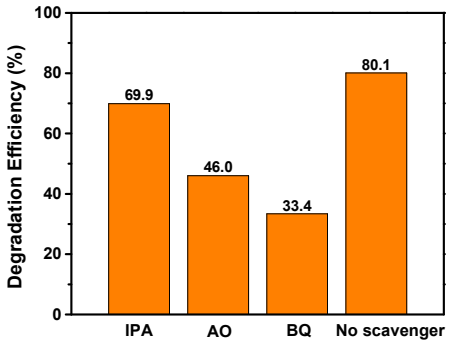

(**c**)

Figure 9. Reactive species trapping experiments: (**a**) effect of quenching agent IPA and AO (observed by UV-Vis spectrophotometry); (**b**) effect of quenching agent BQ (obtained by photoluminescence measurements); (**c**) degradation efficiency.

Various changes in photocatalytic efficiency were observed for the different scavengers. As shown in Figure 9a, in the presence of IPA, the degradation rate moderately decreased compared to the case with no scavenger. The degradation efficiency was reduced from 80.1% to 69.9% (Figure 9c). This observation suggests that •OH radicals only slightly contribute to the photodegradation of levofloxacin. It is not surprising on the basis of the determined edge potential of the valence band of the prepared g-C_3N_4. Moreover, it is in accordance with the results obtained for modified photocatalysts with much higher EVB values [15,16]. The presence of AO resulted in a more appreciable decrease in the degradation rate (Figure 9a) and the efficiency dropped by almost a quarter of the original

performance (to H = 46.0%, Figure 9c). This result indicates that the role of valence-band holes is important in the degradation process. This observation confirms that the adsorption of LEV is indispensable for its interaction with h_{VB}^+. The most significant inhibition effect was observed in the presence of BQ. As shown in Figure 9b, the decrease in the degradation rate was more remarkable, leading to a stronger reduction in the photocatalytic efficiency (to H = 33.4%, Figure 9c). This result unambiguously suggests that $^{\bullet}O_2^-$ plays the most important role in the photocatalytic degradation of LEV. The participation of valence-band holes in the degradation process is less significant but still considerably, while hydroxyl radicals play a minor role in this mechanism.

2.6. Proposed Removal Mechanisms of Levofloxacin by the g-C_3N_4 Photocatalyst

Possible photocatalytic mechanisms for the degradation of LEV have been proposed based on the above quenching experiments and literature reports [17,48–50]. As illustrated in Equations (4)–(11), under sunlight irradiation, g-C_3N_4 was excited to form electron-hole pairs by absorbing light. The potential of the conduction band edge of g-C_3N_4 (E_{CB} = −1.07 V vs. NHE) is more negative than the standard reduction potential of $O_2/^{\bullet}O_2^-$ pair (−0.16 V vs. NHE, pH 7) [39], indicating that the accumulated electrons can reduce O_2 to $^{\bullet}O_2^-$ [51]. The results of the radical trapping experiment showed that $^{\bullet}OH$ played a negligible role in the photocatalytic process, suggesting that degradation of LEV in the valence band is mainly due to the direct reaction with h^+ rather than $^{\bullet}OH$. Furthermore, $^1O_2$ can be generated by the reaction of $^{\bullet}O_2^-$ and h^+, Equations (10)–(12) [18,52]. Finally, ROS ($^{\bullet}O_2^-$, h^+, $^1O_2$, $^{\bullet}OH$) reacted with LEV molecules on the g-C_3N_4 surface, resulting in the decomposition and eventual complete mineralization of LEV, Equation (15). The photocatalytic mechanism of LEV decomposition by g-C_3N_4 catalyst was proposed and is shown in Figure 10.

$$\text{g-}C_3N_4 + h\upsilon \rightarrow \text{g-}C_3N_4\ (e^- + h_{VB}^+) \quad (4)$$

$$O_2 + e^- \rightarrow {}^{\bullet}O_2^- \quad (5)$$

$$O_2 + H^+ + e^- \rightarrow {}^{\bullet}HO_2 \quad (6)$$

$$^{\bullet}HO_2 + {}^{\bullet}HO_2 \rightarrow H_2O_2 \quad (7)$$

$$^{\bullet}O_2^- + 2H^+ + e^- \rightarrow H_2O_2 \quad (8)$$

$$^{\bullet}HO_2 + H^+ + e^- \rightarrow H_2O_2 \quad (9)$$

$$H_2O_2 + h\upsilon \rightarrow 2{}^{\bullet}OH \quad (10)$$

$$H_2O_2 + H^+ + e^- \rightarrow {}^{\bullet}OH + 2H_2O \quad (11)$$

$$h_{VB}^+ + {}^{\bullet}O_2^- \rightarrow {}^1O_2 \quad (12)$$

$$h_{VB}^+ + H_2O \rightarrow {}^{\bullet}OH + H^+ \quad (13)$$

$$h_{VB}^+ + OH^- \rightarrow {}^{\bullet}OH \quad (14)$$

$$^{\bullet}O_2^-/{}^{\bullet}HO_2/{}^{\bullet}OH/{}^1O_2 + \text{LEV} \rightarrow \text{degradation products} \quad (15)$$

LC-MS/MS was used to identify LEV degradation products to further analyze the degradation path of LEV by g-C_3N_4 photocatalyst. Mass spectra of levofloxacin in the photodegradation experiments (i) light-off for 30 min, (ii) light-on for 40 min, and (iii) light-on for 120 min were recorded. With the levofloxacin solution in the dark, molecular ion peaks $[M+H]^+$ (m/z = 362) were initially produced (Figure S2a). During the degradation process, intermediates were formed (Figure S2b). Molecular ion peaks undergo N-methyl piperazine ring breaking reaction to form P1 (m/z = 265) and an intermediate at m/z = 99. P2 (m/z = 218) and P3 (m/z = 217) intermediates appeared as products of decarboxylation and quinolone ring opening reactions. Meanwhile, the loss of $-C_3OH_2$ and hydroxylation occurs on P3, producing P4 (m/z = 170). P4 was further defluorinated and demethylated to form P5 (m/z = 122). Subsequently, intermediate P5 product might continue to be broken

into small molecules as well as mineralization product (main peaks at $m/z < 50$ region as seen from Figure S2c).

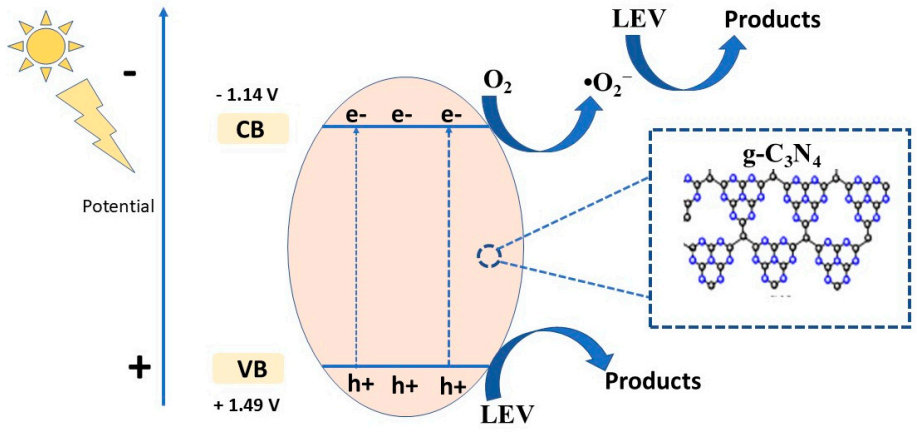

Figure 10. Photocatalytic mechanism of levofloxacin by g-C3N4 photocatalyst.

The intermediate and degradation paths are proposed as shown in Scheme 1. The degradation of LEV is mainly by piperazine ring breaking and opening, quinolone ring opening, defluorination, demethylation, decarboxylation/carboxylation, and hydroxylation processes as detailed above [40].

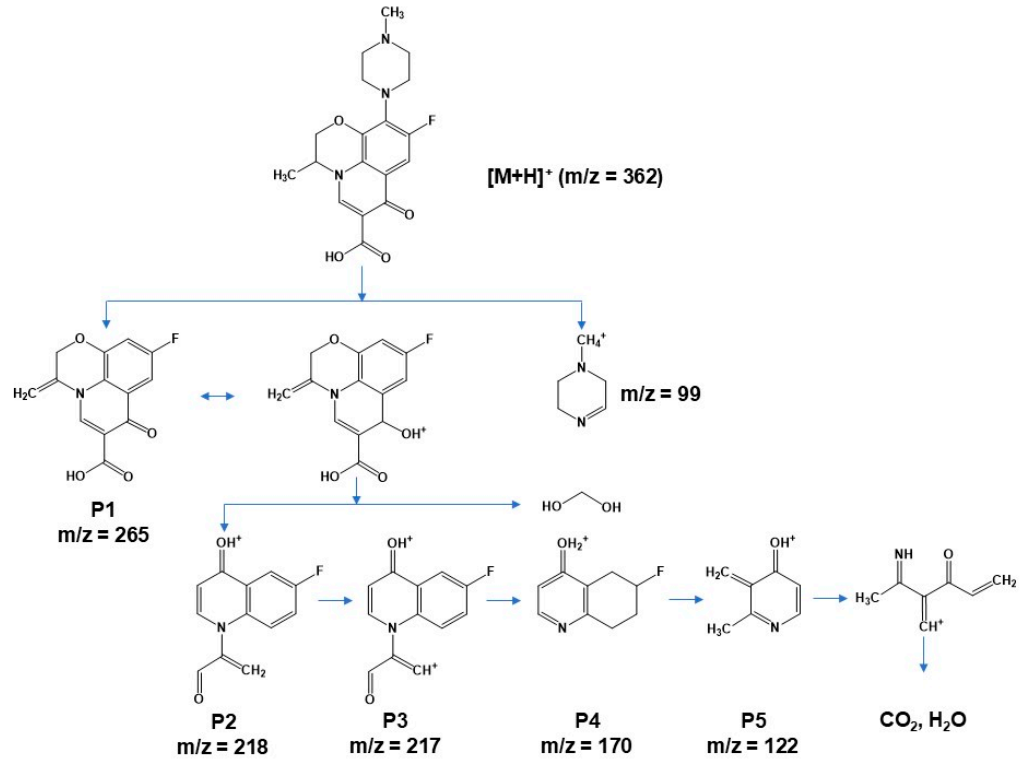

Scheme 1. The proposed degradation pathway of LEV.

3. Materials and Methods

3.1. Reagents

Thiourea (99%) and ethanol (99%) were obtained from Merck, Darmstadt, Germany. p-benzoquinone (99.0%, Xiya Reagent (Xiya Chemicals Co., Ltd., Shandong, China)), ammoniumoxalate monohydrate (99.5%), and isopropyl alcohol (99.7%) were purchased from Xilong, Shantou, China. Sodium hydroxide (NaOH, 99.8%) and hydrochloric acid (HCl, 36–38%) were obtained from Sigma-Aldrich (Burlington, MA, USA). Levofloxacin

($C_{18}H_{20}FN_3O_4$, LEV, 97.0%) was purchased from Vietnam National Institute of Drug Quality Control. All chemicals have been used without purification.

3.2. Preparation of g-C_3N_4

g-C_3N_4 was prepared by thermal polymerization of thiourea, an abundant nitrogen-rich precursor [1–3]. Typically, 3 g of thiourea was put into a porcelain crucible with a cover, then calcinated at 550 °C for 4 h at a heating rate of 2 °C min^{-1} under air atmosphere. After calcination, the samples were washed with deionized water and ethanol several times and dried at 60 °C. g-C_3N_4 was obtained, ground, and collected for further experiments. Since thiourea contains sulfur, the elemental composition of the product was checked by EDS measurements. The results showed that the whole sulfur content of the precursor had been removed during the preparation process (Figure S3).

3.3. Sample Characterization

The samples prepared were characterized by X-ray diffraction (XRD, Malvern PANalytical, Aeris, Almelo, The Netherlands) and scanning electron microscopy (SEM, NanoSEM 450 FEI, Eindhoven, The Netherlands) combined with a TEAM Apollo XL energy dispersive spectroscopy (EDS, EDAX, Cambridge, UK). UV-Vis spectra were recorded by an Agilent 8453 spectrophotometer (Santa Clara, CA, USA), while diffuse reflectance spectra were measured on a Carry 5000 UV-Vis-NIR equipment (Santa Clara, CA, USA). Luminescence was measured by a F-4700 spectrofluorometer (Hitachi, Tokyo, Japan). The reaction intermediates were analyzed by SCIEX Exion LC 20AD LC-MS/MS system (SCIEX, Framingham, MA, USA): column Agilent Eclipse Plus C18 (2.1 × 50 mm, ID 3.5 μm) and detector AB SCIEX Triple Quad 6500+.

3.4. Point-Zero Charge and Surface Charge Determination

It has been reported that the pH-drift method can be used to determine the pH of zero charge and surface charge [4,5]. In this study, it was measured on the basis of the work by Mahmood et. al. [53]. 100 mL LEV solution (10 mg/L) was adjusted to pH (2, 4, 6, 8, 10, 12) in test tubes at room temperature using NaOH and HCl (0.1 M) and the initial pH was recorded. Then 50 mg of g-C_3N_4 photocatalyst was added and stirred for 24 h under dark conditions. The suspension was removed from the tube, the pH was measured, and the final pH was recorded.

3.5. Photocatalytic Degradation Experiments

The catalytic performance of g-C_3N_4 was evaluated by the degradation of LEV under the irradiation of a 500-W Hg-lamp, as a simulated solar source. The emission spectrum of the light source is shown in Figure S4. The intensity of radiation was 26 lm W^{-1}. The experimental procedure was as follows: 50 mg of g-C_3N_4 was dispersed in a 100 mL LEV (10 mg L^{-1}) solution, and subsequently, the suspension was sonicated for about 3 min. Prior to the irradiation, the mixture was kept for 30 min in the dark with stirring at room temperature to obtain an adsorption-desorption equilibrium. At each given time interval (10 min), 3 mL of the solution was collected and filtered with a filter (0.22 μm PTFE membrane) to remove the catalyst. The concentration of LEV was examined by UV-Vis spectrophotometry in the wavelength range from 200 to 400 nm. The photocatalytic degradation efficiency was calculated according to the following equation (Equation (16)).

$$H = \frac{C_0 - C_t}{C_0} = \frac{A_0 - A_t}{A_0} \quad (16)$$

where, C_t and A_t—concentration and absorbance of the solution at time t; C_0 and A_0— adsorption/desorption equilibrium concentration and absorbance of the solution at time t_0.

A simplified pseudo-first-order kinetic model of Langmuir–Hinshewood (Equation (17)) was used to explore the kinetic of the photocatalysis process.

$$ln\frac{C_0}{C_t} = k_{app}t = kKt \quad (17)$$

where C—concentration of the antibiotic (mg L^{-1}), t—time for degradation (min), k_{app}—apparent rate constant (min^{-1}), k—reaction rate constant (min^{-1}), and K—adsorption coefficient of the antibiotic over catalyst particles.

3.6. Radical Trapping Experiments

Isopropyl alcohol (IPA, 5.0×10^{-3} M), benzoquinone (BQ, 2.5×10^{-4} M) and ammonium oxalate (5.0×10^{-3} M) were used as scavengers for trapping the photogenerated $^{\bullet}OH$, $^{\bullet}O_2^-$, and holes radicals during the degradation of LEV.

3.7. Intermediates Identification

The intermediates generated during the photocatalytic degradation of levofloxacin solution were further investigated by LC-MS/MS measurement. The mass spectra of the photodegradation products are shown in Figure S2. They were used to propose the photodegradation route of levofloxacin.

3.8. Recycling Experiments

To investigate the reusability of the g-C_3N_4, consecutive experiments for degradation of LEV were carried out in four cycles. After each cycle, the catalyst was recovered by filtration and washed several times with distilled water and ethanol then dried at 60 °C for 10 h.

4. Conclusions

The g-C_3N_4 photocatalyst was successfully synthesized from thiourea precursor at a calcination temperature of 550 °C. The prepared catalyst was characterized by XRD and SEM. The experimental parameters, including the initial pH solution, catalyst dose, and initial LEV concentration, greatly influence the photodegradation of LEV antibiotics. The disappearance of LEV followed the Langmuir-Hinshelwood (L-H) kinetic model. Radical scavenger experiments confirmed that $^{\bullet}O_2^-$ and h^+ played significant roles during the photocatalytic degradation of LEV. Optimized reaction conditions lead to the conclusion that a g-C_3N_4 and a use of 0.5 g/L photocatalyst concentration and 10 mg L^{-1} LEV solution at pH 5 eliminate 80.1% LEV within a 60-min irradiation with solar-simulated light. Based on the identification of intermediates using LC-MS/MS, the photocatalytic degradation pathways of LEV were proposed. The present catalyst exhibits good stability even after four cycles. The EF factor indicates that g-C_3N_4 can be used as a potential photocatalyst for antibiotic degradation.

Supplementary Materials: The following supporting information can be downloaded at: https://www.mdpi.com/article/10.3390/catal14110837/s1, Figure S1. (a) DR/UV-Vis spectra; (b) energy bandgap determination by the Tauc plots. Figure S2. Mass spectra of levofloxacin in the photodegradation experimental: (a) light-off for 30 minutes, (b) light-on for 40 minutess and (c) light-on for 120 minutes. Figure S3. EDS measurement of the prepared g-C_3N_4. Figure S4. Profile of the 500-W Hg-lamp (Philips Lighting product data).

Author Contributions: Conceptualization, T.N.X.; methodology, T.N.X. and O.H.; software, T.N.X.; validation, D.N.T., C.L.T., T.M.T., T.L.D. and T.N.D.; formal analysis, T.N.X. and O.H.; investigation, D.N.T., C.L.T., T.M.T., T.L.D. and T.N.D.; resources, T.N.X. and O.H.; data curation, D.N.T., C.L.T., T.M.T., T.L.D. and T.N.D.; writing—original draft preparation, T.N.X. and O.H.; writing—review and editing, T.N.X. and O.H.; visualization, T.N.X. and O.H.; supervision, T.N.X. and O.H.; project administration, T.N.X. and O.H.; funding acquisition, T.N.X. and O.H. All authors have read and agreed to the published version of the manuscript.

Funding: This work was supported by the National Research, Development, and Innovation Office of Hungary in the frame of the bilateral Hungarian-Vietnamese S&T Co-operation Program (project code 2019-2.1.12-TÉT_VN-2020-00009 and NĐT/HU/22/21) and by the Ministry for Innovation and Technology of Hungary from the National Research, Development and Innovation Fund, financed under the 2021 Thematic Excellence Program funding scheme (grant number TKP2021-NKTA-21).

Data Availability Statement: The data presented in this study are available on request from the corresponding author. The data are not publicly available due to privacy.

Conflicts of Interest: The authors declare no conflicts of interest.

References

1. Hong, Y.; Liu, E.; Shi, J.; Lin, X.; Sheng, L.; Zhang, M.; Wang, L.; Chen, J. A direct one-step synthesis of ultrathin g-C_3N_4 nanosheets from thiourea for boosting solar photocatalytic H_2 evolution. *Int. J. Hydrog. Energy* **2019**, *44*, 7194–7204. [CrossRef]
2. Wang, H.; Sun, Z.; Li, Q.; Tang, Q.; Wu, Z. Surprisingly advanced CO_2 photocatalytic conversion over thiourea derived g-C_3N_4 with water vapor while introducing 200–420 nm UV light. *J. CO2 Util.* **2016**, *14*, 143–151. [CrossRef]
3. Paul, D.R.; Sharma, R.; Nehra, S.P.; Sharma, A. Effect of calcination temperature, pH and catalyst loading on photodegradation efficiency of urea derived graphitic carbon nitride towards methylene blue dye solution. *RSC Adv.* **2019**, *9*, 15381–15391. [CrossRef] [PubMed]
4. Noh, J.S.; Schwarz, J.A. Estimation of the point of zero charge of simple oxides by mass titration. *J. Colloid Interface Sci.* **1989**, *130*, 157–164. [CrossRef]
5. Zhu, P.; Luo, D.; Liu, M.; Duan, M.; Lin, J.; Wu, X. Flower-globular BiOI/$BiVO_4$/g-C_3N_4 with a dual Z-scheme heterojunction for highly efficient degradation of antibiotics under visible light. *Sep. Purif. Technol.* **2022**, *297*, 121503. [CrossRef]
6. Czyrski, A. Analytical Methods for Determining Third and Fourth Generation Fluoroquinolones: A Review. *Chromatographia* **2017**, *80*, 181–200. [CrossRef]
7. Sousa, J.; Alves, G.; Fortuna, A.; Falcão, A. Analytical methods for determination of new fluoroquinolones in biological matrices and pharmaceutical formulations by liquid chromatography: A review. *Anal. Bioanal. Chem.* **2012**, *403*, 93–129. [CrossRef]
8. Van, T.T.; Minejima, E.; Chiu, C.A.; Butler-Wu, S.M. Don't Get Wound Up: Revised Fluoroquinolone Breakpoints for Enterobacteriaceae and Pseudomonas aeruginosa. *J. Clin. Microbiol.* **2019**, *57*, e02072-18. [CrossRef]
9. Fish, D.N.; Chow, A.T. The Clinical Pharmacokinetics of Levofloxacin. *Clin. Pharmacokinet.* **1997**, *32*, 101–119. [CrossRef]
10. Goulart, L.A.; Moratalla, A.; Lanza, M.R.V.; Saez, C.; Rodrigo, M.A. Photocatalytic performance of Ti/MMO/ZnO at degradation of levofloxacin: Effect of pH and chloride anions. *J. Electroanal. Chem.* **2021**, *880*, 114894. [CrossRef]
11. Guo, P.; Hu, X. Co, Fe co-doped g-C_3N_4 composites as peroxymonosulfate activators under visible light irradiation for levofloxacin degradation: Characterization, performance and synergy mechanism. *Colloids Surf. A Physicochem. Eng. Asp.* **2022**, *648*, 129423. [CrossRef]
12. Guo, P.; Hu, X. ZIF-derived $CoFe_2O_4$/Fe_2O_3 combined with g-C_3N_4 as high-efficient photocatalysts for enhanced degradation of levofloxacin in the presence of peroxymonosulfate. *J. Alloys Compd.* **2022**, *914*, 165338. [CrossRef]
13. Zhao, J.; Cao, X.; Bai, Y.; Chen, J.; Zhang, C. Simple synthesis of $CaTiO_3$/g-C_3N_4 heterojunction for efficient photodegradation of methylene blue and levofloxacin. *Opt. Mater.* **2023**, *135*, 113239. [CrossRef]
14. Li, F.; Zhu, P.; Wang, S.; Xu, X.; Zhou, Z.; Wu, C. One-pot construction of Cu and O co-doped porous g-C3N4 with enhanced photocatalytic performance towards the degradation of levofloxacin. *RSC Adv.* **2019**, *9*, 20633–20642. [CrossRef]
15. Gupta, G.; Kaur, A.; Sinha, A.S.K.; Kansal, S.K. Photocatalytic degradation of levofloxacin in aqueous phase using Ag/AgBr/BiOBr microplates under visible light. *Mater. Res. Bull.* **2017**, *88*, 148–155. [CrossRef]
16. Kaur, A.; Kansal, S.K. Bi_2WO_6 nanocuboids: An efficient visible light active photocatalyst for the degradation of levofloxacin drug in aqueous phase. *Chem. Eng. J.* **2016**, *302*, 194–203. [CrossRef]
17. Prabavathi, S.L.; Saravanakumar, K.; Park, C.M.; Muthuraj, V. Photocatalytic degradation of levofloxacin by a novel Sm_6WO_{12}/g-C_3N_4 heterojunction: Performance, mechanism and degradation pathways. *Sep. Purif. Technol.* **2021**, *257*, 117985. [CrossRef]
18. Wang, F.; Feng, Y.; Chen, P.; Wang, Y.; Su, Y.; Zhang, Q.; Zeng, Y.; Xie, Z.; Liu, H.; Liu, Y.; et al. Photocatalytic degradation of fluoroquinolone antibiotics using ordered mesoporous g-C_3N_4 under simulated sunlight irradiation: Kinetics, mechanism, and antibacterial activity elimination. *Appl. Catal. B Environ.* **2018**, *227*, 114–122. [CrossRef]
19. Martin, D.J.; Qiu, K.; Shevlin, S.A.; Handoko, A.D.; Chen, X.; Guo, Z.; Tang, J. Highly Efficient Photocatalytic H_2 Evolution from Water using Visible Light and Structure-Controlled Graphitic Carbon Nitride. *Angew. Chem. Int. Ed.* **2014**, *53*, 9240–9245. [CrossRef]
20. Zhang, Y.; Liu, J.; Wu, G.; Chen, W. Porous graphitic carbon nitride synthesized via direct polymerization of urea for efficient sunlight-driven photocatalytic hydrogen production. *Nanoscale* **2012**, *4*, 5300. [CrossRef]
21. Dong, F.; Wu, L.; Sun, Y.; Fu, M.; Wu, Z.; Lee, S.C. Efficient synthesis of polymeric g-C_3N_4 layered materials as novel efficient visible light driven photocatalysts. *J. Mater. Chem.* **2011**, *21*, 15171. [CrossRef]
22. Yang, Y.; Zhang, Q.; Zhang, R.; Ran, T.; Wan, W.; Zhou, Y. Compressible and Recyclable Monolithic g-C_3N_4/Melamine Sponge: A Facile Ultrasonic-Coating Approach and Enhanced Visible-Light Photocatalytic Activity. *Front. Chem.* **2018**, *6*, 156. [CrossRef]

23. Das, D.; Banerjee, D.; Das, B.; Das, N.S.; Chattopadhyay, K.K. Effect of cobalt doping into graphitic carbon nitride on photo induced removal of dye from water. *Mater. Res. Bull.* **2017**, *89*, 170–179. [CrossRef]
24. Komatsu, T. Prototype carbon nitrides similar to the symmetric triangular form of melon. *J. Mater. Chem.* **2001**, *11*, 802–803. [CrossRef]
25. Komatsu, T. The First Synthesis and Characterization of Cyameluric High Polymers. *Macromol. Chem. Phys.* **2001**, *202*, 19–25. [CrossRef]
26. Machín, A.; Cotto, M.; Duconge, J.; Arango, J.C.; Morant, C.; Pinilla, S.; Soto-Vázquez, L.; Resto, E.; Márquez, F. Hydrogen production via water splitting using different Au@ZnO catalysts under UV–vis irradiation. *J. Photochem. Photobiol. A Chem.* **2018**, *353*, 385–394. [CrossRef]
27. Rameel, M.I.; Wali, M.; Al-Humaidi, J.Y.; Liaqat, F.; Khan, M.A. Enhanced photocatalytic degradation of levofloxacin over heterostructured C_3N_4/Nb_2O_5 system under visible light. *Heliyon* **2023**, *9*, e20479. [CrossRef]
28. Luo, Y.; Zhu, Y.; Han, Y.; Ye, H.; Liu, R.; Lan, Y.; Xue, M.; Xie, X.; Yu, S.; Zhang, L.; et al. g-C_3N_4-based photocatalysts for organic pollutant removal: A critical review. *Carbon Res.* **2023**, *2*, 14. [CrossRef]
29. Zhong, X.; Ji, M.; Wu, W.; Lu, C.; Liu, W.; Jiang, F. Enhanced Degradation of Levofloxacin through Visible-Light-Driven Peroxymonosulfate Activation over $CuInS_2$/g-C_3N_4 Heterojunctions. *Nanomaterials* **2023**, *14*, 74. [CrossRef]
30. Zhang, X.; Tian, Y.; Zhou, L.; Wang, L.; Zhang, J.; Liu, Y.; Lei, J. Efficient degradation of levofloxacin using a g-C_3N_4@glucose-derived carbon catalyst with adjustable N content via peroxymonosulfate activation. *Chemosphere* **2023**, *314*, 137684. [CrossRef]
31. Yan, S.C.; Li, Z.S.; Zou, Z.G. Photodegradation Performance of g-C_3N_4 Fabricated by Directly Heating Melamine. *Langmuir* **2009**, *25*, 10397–10401. [CrossRef] [PubMed]
32. Wang, X.; Chen, X.; Thomas, A.; Fu, X.; Antonietti, M. Metal-Containing Carbon Nitride Compounds: A New Functional Organic–Metal Hybrid Material. *Adv. Mater.* **2009**, *21*, 1609–1612. [CrossRef]
33. Negro, P.; Cesano, F.; Casassa, S.; Scarano, D. Combined DFT-D3 Computational and Experimental Studies on g-C_3N_4: New Insight into Structure, Optical, and Vibrational Properties. *Materials* **2023**, *16*, 3644. [CrossRef] [PubMed]
34. Pattnaik, S.; Rai, V.K. Insight into the spectroscopic and thermometric properties of titanate phosphors via a novel co-excited laser system. *Mater. Sci. Eng. B* **2021**, *272*, 115318. [CrossRef]
35. Xuan, T.N.; Thi, D.N.; Ngoc, T.N.; Quoc, K.D.; Németh, M.; Mukhtar, S.; Horváth, O. Effect of Ruthenium Modification of g-C_3N4 in the Visible-Light-Driven Photocatalytic Reduction of Cr(VI). *Catalysts* **2023**, *13*, 964. [CrossRef]
36. Nguyen Xuan, T.; Nguyen Thi, D.; Tran Thuong, Q.; Nguyen Ngoc, T.; Dang Quoc, K.; Molnár, Z.; Mukhtar, S.; Szabó-Bárdos, E.; Horváth, O. Effect of Copper-Modification of g-C_3N_4 on the Visible-Light-Driven Photocatalytic Oxidation of Nitrophenols. *Molecules* **2023**, *28*, 7810. [CrossRef]
37. Machín, A.; Fontánez, K.; Duconge, J.; Cotto, M.C.; Petrescu, F.I.; Morant, C.; Márquez, F. Photocatalytic Degradation of Fluoroquinolone Antibiotics in Solution by Au@ZnO-rGO-gC_3N_4 Composites. *Catalysts* **2022**, *12*, 166. [CrossRef]
38. Cao, J.; Han, F.; Wang, L.; Huang, X.; Cao, Y.; He, P.; Yang, H.; Chen, J.; Li, H. Ru/g-C_3N_4 as an efficient catalyst for selective hydrogenation of aromatic diamines to alicyclic diamines. *RSC Adv.* **2020**, *10*, 16515–16525. [CrossRef]
39. Li, J.; Jiang, M.; Zhou, H.; Jin, P.; Cheung, K.M.C.; Chu, P.K.; Yeung, K.W.K. Vanadium Dioxide Nanocoating Induces Tumor Cell Death through Mitochondrial Electron Transport Chain Interruption. *Glob. Chall.* **2019**, *3*, 1800058. [CrossRef]
40. Lu, X.; Wu, L.; Liang, L.; Liu, D.; Chen, Y.; Zeng, Y.; Zhong, M.; Jia, B. Levofloxacin degradation by porous Co_x/CN activated peroxymonosulfate: Investigation of efficiency, mechanism, and degradation pathways. *J. Water Process Eng.* **2023**, *56*, 104427. [CrossRef]
41. Xing, Z.; Wang, Z.; Chen, W.; Zhang, M.; Fu, X.; Gao, Y. Degradation of levofloxacin in wastewater by photoelectric and ultrasonic synergy with TiO_2/g-C_3N_4@AC combined electrode. *J. Environ. Manag.* **2023**, *330*, 117168. [CrossRef] [PubMed]
42. Li, X.; Chen, T.; Qiu, Y.; Zhu, Z.; Zhang, H.; Yin, D. Magnetic dual Z-scheme g-C_3N_4/$BiVO_4$/$CuFe_2O_4$ heterojunction as an efficient visible-light-driven peroxymonosulfate activator for levofloxacin degradation. *Chem. Eng. J.* **2023**, *452*, 139659. [CrossRef]
43. Ahmed, S.; Rasul, M.G.; Martens, W.N.; Brown, R.; Hashib, M.A. Advances in Heterogeneous Photocatalytic Degradation of Phenols and Dyes in Wastewater: A Review. *Water Air Soil Pollut.* **2011**, *215*, 3–29. [CrossRef]
44. Yan, H.; Luo, M.; Chen, Q.; Jeong, T.; Zhang, J.; Wang, L. Efficacy and mechanism of chemical-free VUV/UV process for oxytetracycline degradation: Continuous-flow experiment and CFD modeling. *Chem. Eng. J. Adv.* **2020**, *4*, 100059. [CrossRef]
45. Kohantorabi, M.; Moussavi, G.; Oulego, P.; Giannakis, S. Synthesis of a novel, ternary AgI/CeO_2@g-C_3N_4 nanocomposite with exceptional stability and reusability for visible light-assisted photocatalytic reduction of hexavalent chromium. *Appl. Surf. Sci.* **2021**, *555*, 149692. [CrossRef]
46. Balakumar, V.; Selvarajan, S.; Baishnisha, A.; Kathiresan, S. In-situ growth of TiO_2@B-doped g-C_3N_4 core-shell nanospheres for boosts the photocatalytic detoxification of emerging pollutants with mechanistic insight. *Appl. Surf. Sci.* **2022**, *577*, 151924. [CrossRef]
47. Singh, S.; Sharma, N.; Sehrawat, P.; Kansal, S.K. Solar-light-driven photocatalytic degradation of pharmaceutical pollutants utilizing 2D g-C3N4/BiOCl composite. *Environ. Toxicol. Pharmacol.* **2023**, *99*, 104110. [CrossRef]
48. Liu, W.; Li, Z.; Kang, Q.; Wen, L. Efficient photocatalytic degradation of doxycycline by coupling α-Bi_2O_3/g-C_3N_4 composite and H_2O_2 under visible light. *Environ. Res.* **2021**, *197*, 110925. [CrossRef]
49. Chen, C.; Xie, M.; Kong, L.; Lu, W.; Feng, Z.; Zhan, J. Mn_3O_4 nanodots loaded g-C_3N_4 nanosheets for catalytic membrane degradation of organic contaminants. *J. Hazard. Mater.* **2020**, *390*, 122146. [CrossRef]

50. He, Y.; Ma, Z.; Junior, L.B. Distinctive binary g-C_3N_4/MoS_2 heterojunctions with highly efficient ultrasonic catalytic degradation for levofloxacin and methylene blue. *Ceram. Int.* **2020**, *46*, 12364–12372. [CrossRef]
51. Zhang, C.; Ouyang, Z.; Yang, Y.; Long, X.; Qin, L.; Wang, W.; Zhou, Y.; Qin, D.; Qin, F.; Lai, C. Molecular engineering of donor-acceptor structured g-C_3N_4 for superior photocatalytic oxytetracycline degradation. *Chem. Eng. J.* **2022**, *448*, 137370. [CrossRef]
52. Wang, F.; Wang, Y.; Feng, Y.; Zeng, Y.; Xie, Z.; Zhang, Q.; Su, Y.; Chen, P.; Liu, Y.; Yao, K.; et al. Novel ternary photocatalyst of single atom-dispersed silver and carbon quantum dots co-loaded with ultrathin g-C_3N_4 for broad spectrum photocatalytic degradation of naproxen. *Appl. Catal. B Environ.* **2018**, *221*, 510–520. [CrossRef]
53. Mahmood, T.; Saddique, M.T.; Naeem, A.; Westerhoff, P.; Mustafa, S.; Alum, A. Comparison of Different Methods for the Point of Zero Charge Determination of NiO. *Ind. Eng. Chem. Res.* **2011**, *50*, 10017–10023. [CrossRef]